



# Synthesis of Fe–Al Intermetallic by Mechanical Alloying Process

Vivek Kumar Jain<sup>1</sup> · Manoj Kumar Yadav<sup>2</sup> · Arshad Noor Siddiquee<sup>3</sup> ·  
Zahid Akhtar Khan<sup>3</sup> · Chaitanya Sharma<sup>4</sup>

Received: 26 November 2021 / Accepted: 24 February 2022 / Published online: 25 April 2022  
© The Institution of Engineers (India) 2022

**Abstract** In the present work, mechanical alloying (MA) of iron and aluminum powder has been performed by planetary ball mills. Milling balls of different sizes 5, 15, and 20 mm in diameter were used for the milling medium. MA was done for different duration of time to refine the grain and crystallite size of the powder. Structural and phase changes occurred in the powder mixture on account of MA. The structural evolution and morphological analysis of the Fe<sub>60</sub>Al<sub>40</sub> powder during MA were analyzed using X-ray diffraction and scanning electron microscope. MA of elemental aluminum (Al) and iron (Fe) powder results in the development of Fe(Al)-supersaturated solid solution phase. The effect of the MA on average grain size, mean crystallite size, and lattice strain was assessed. For disordered Fe(Al) solid solution milled for 40 h, these values were 10 μm, 18.2 nm, and 0.44%, respectively.

**Keywords** Mechanical alloying (MA) · Intermetallic compound · Aluminum · Iron aluminides

## Introduction

An intermetallic compound (IMC) is a compound in solid-state having an extended variety of ordered structures demonstrating extraordinary metallic bonding. IMCs are fabricated from two or more metallic materials and generating a novel phase with a similar configuration, crystalline structure, and properties. Nowadays, IMCs are gaining wide prominence owing to the unique blend of desirable properties such as outstanding high-temperature strength, heat resistant, high corrosion, and oxidation resistance [1]. The FeAl-based intermetallic compounds are found to possess moderately high electrical resistance, lower thermal conductivity, excessive strength-to-weight ratio, moderate strength at intermediary temperature, and outstanding corrosion resistance at raised temperatures in various environments such as oxidizing, carburizing, and sulfidizing environment (H<sub>2</sub>S and SO<sub>2</sub> gases) [2, 3]. These special characteristics make FeAl very promising candidates for structural purposes at raised temperatures in challenging environments [4, 5]. Due to lightweight and low density, they may be considered as engineering material to substitute stainless steel, Fe-, and Ni-based super alloys [6]. However, like all IMCs, FeAl compounds have limited ductility at room temperature and reduced mechanical strength beyond 600 °C [7].

Mechanical alloying (or MA as it is also termed as) is an efficacious approach to produce nano-crystalline alloys. Several published works on MA of Fe- 50% Al [8–13] report that a disordered Fe(Al) solid solution was obtained after milling. Similarly, Morris-Muñoz et al. [14] reported that a partially ordered Fe(Al) solid solution phase was attained after MA of Fe- 50% Al. In all the reported work, it was emphasized that supplementary heat treatment was compulsory to acquire the fully ordered structure after the

✉ Chaitanya Sharma  
cs.me@bitsindri.ac.in

<sup>1</sup> Department of Mechanical Engineering, IMS Engineering College, Ghaziabad, UP 201013, India

<sup>2</sup> Department of Mechanical Engineering, Inderprastha Engineering College, Ghaziabad, UP 201010, India

<sup>3</sup> Department of Mechanical Engineering, Jamia Millia Islamia, New Delhi 110025, India

<sup>4</sup> Department of Mechanical Engineering, BIT, Sindri, Dhanbad 828123, India

MA. MA was developed by John S. Benjamin and his colleagues at the Paul D. Merica Research Laboratory of the International Nickel Company (INCO) in the year about 1966 to developed nickel-based oxide dispersion-strengthened (ODS) super alloys [15].

MA shows a special eminence of prolonged solid solubility of incompatible stages at equipose [16] and gives rise to an alloy development by a solid-state response by severe plastic deformation (SPD) through ball milling. It creates added versatile and constructive technique for alloying and synthesizing the different powder mixture. MA attracts the researchers; as there is no loss of material, better homogeneity of nano-crystalline material, and synthesized different intermetallic phases [17]. The materials produced by MA display superior properties as compared to conventional ones. It is a remarkable and significant process to create oxide dispersion-strengthened alloys (ODS), composites, nano-crystalline material, and amorphous phases powders which were very difficult to fabricated by a conventional method such as melting [18]. Thus, MA allows us to produce such alloying components that have a vast difference in their melting temperature.

The MA is a solid-state technique and usually performed at room temperature, though there is some rise of temperature arises during the process. During MA, repeated fracturing and the cold forging of component particles happen due to high-energy collision as shown in Fig. 1. The impact of balls on the alloying mixture during the planetary motion is accountable for the mixing, crushing, and fracturing of powder [19]. Constituent powder particles pierce each other, become plastically deformed, and result in inhomogeneity in structure with prolongs milling [20]. MA commonly performed in an inert environment to avoid oxidation and contamination of powders [21, 22].

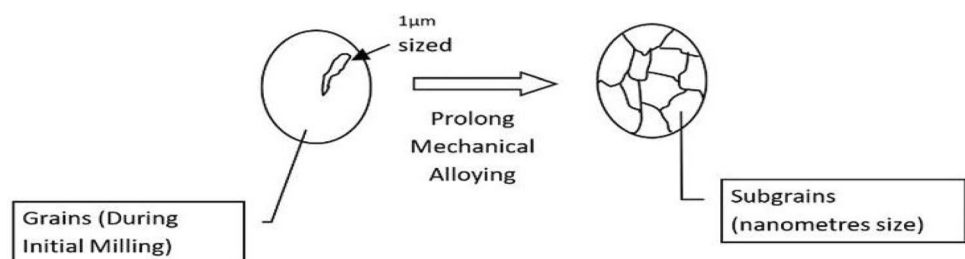
During the process, a small amount of process control agent (PCA) is added with the alloyed material. PCA avoids cold welding of powder either with the balls or with the wall of the bowl and reduced the possibility of fracturing powders into too many small parts. The PCAs also affect the alloying process. The chemical affinity between chosen PCA and the material to be processed sometimes may introduce objectionable material in the MAed powder mixture such as oxygen, nitrogen, and hydrogen which

produces new unsolicited phases and affect the chemical configuration of mechanically alloyed material. So, special care should be taken in the proper selection of PCAs [24, 25]. Depending upon the process, researchers used different types of PCA such as calcium, magnesium, magnesium master alloys, stearic acid, benzene, ethyl alcohol, and methanol.

To avoid oxidation and contamination of newly and freshly fractured surfaces during milling due to an increase in the oxygen content while MA [26], an inert atmosphere is provided. Argon, helium, nitrogen, and air as the milling atmosphere have been widely used during the MA. The weight of the balls to the weight of powder is called BPR or charge ratio (CR), also a significant process variable in the alloying process. Different investigators varied these values from 1:1 [27] to 220:1 [28] in their research. But the value of BPR of around 5:1–10:1 is effective [29]. Small BPR value reduces the effective movement of the balls, hinders their path, and ultimately decreases the alloying rate, whereas high BPR value reduces the frequency of collision between powder and balls and deteriorates the alloying medium. Therefore, the required quantity of the powder mixture and the balls (BPR) for filling the bowl is also very vital. Apart from them, numerous other factors affect the alloying process such as mills type, starting size of powder, bowl and balls material, milling time, and temperature of milling [15, 30–32]. MA was performed via various types of high-energy mills. A few of them are SPEX shaker mills, tumbler mills, attritor mills, planetary mills, and commercial mills. Apart from that numerous mills have been evolved for specific tasks in recent years and various innovative mills are in progress [33].

MA has been recognized as a controlled powder processing technique capable of creating fine microstructure metal composites. It is observed that the shape of powder changes from flaky to semi-rounded shape during the process. It is a potential method to developed stable (equilibrium) and metastable (non-equilibrium) supersaturated solid solutions from mixed powder. Owing to the occurrence of fine dispersoids during the MA, significant improvement has been observed in mechanical properties, creep resistance, and strengthening alloys and super alloys [19, 33].

**Fig. 1** Rupturing of the particle during MA. Yadav et al. [23]



This study was performed to witness the variations in microstructural behavior of the mechanically alloyed (MAed) Fe<sub>60</sub>Al<sub>40</sub> powder under mixed diameter balls for different duration of time in a controlled environment and the formation of new phases. In the previous works, researcher have reported the similar works but in most of the reported work, single ball size was used as a process variable. Therefore, effort has been made to use mixed diameter balls as a process variable. And further, obtained MAed powder will be used as reinforcement for friction stir processing (FSP). The study reflects the behavior of intermetallic formation with the change of process time during mechanical alloying. The obtained results will be helpful for other researchers and material experts to form novel intermetallic using solid-state alloying, i.e., mechanical alloying process.

## Experimental Details

Elemental iron and aluminum powders having a purity of 99% with an average size of 35 and 30 μm, respectively, were blended in a ratio of Fe<sub>60</sub>Al<sub>40</sub>. MA of this mixture was done in a planetary ball mill at a uniform operating speed of 195 rpm for a period of 40 h, in inert argon gas to avoid the oxidation of the mixture throughout the milling process. 2.5% stearic acid (CH<sub>3</sub>(CH<sub>2</sub>)<sub>16</sub>COOH) as PCA was added with the powder to reduce the chances of sticking and welding of powder with the ball and bowl during milling. The Fe<sub>60</sub>Al<sub>40</sub> powder mixture was placed in the hardened steel bowl of capacity 250 ml. Hardened steel balls of mixed diameters (5, 15, and 20 mm) were used as a milling medium. The reason for selecting milling balls with different sizes was to minimize the amount of cold welding and less adhesion of particles on the surfaces of the milling bowl and balls [34]. Also it was mentioned in the literature that the highest collision energy can be obtained if balls with different diameters were used [35]. Then powders and balls mixture were placed in the bowl with BPR of about 10:1 and closed with the “O” band mounted cap. After every 25 min, the milling process was stopped for 10 min to avoid the rise in temperature of the bowl and the powder mixture. Table 1 presents the processing factors which were adopted during MA.

As a precaution, to prevent the formation of oxides during the process, after every 10 h pure Argon gas was eradicated into the bowl. Samples were taken out from the bowl after each 10 h of run and kept in airtight bottles for structural evolution and morphological analysis.

The morphological change in the mechanically alloyed powder for the different duration was inspected by an LEO-435VP scanning electron microscope (SEM). Structural development and phase transformation were

evaluated by X-ray diffraction (XRD). XRD of the milled powders was examined under Bruker-D8 Advance X-ray diffraction machine with Cu Kα1 radiation ( $\lambda = 1.5409 \text{ \AA}$ ) from 25° to 85° in  $2\theta$  range with a step size of 0.0288° because at lower angle, peaks of weak intensity were discovered in the respective spectrum.

## Results and Discussion

Figure 2a and b represents the SEM images of the starting iron (Fe) and aluminum (Al) powder. Fe grains are irregular and acicular in shape and with a wide range of sizes. Smaller grain sizes are nearly equal to 18 μm, whereas very large grain sizes have approximately equaled to 45 μm with an average size of 35 μm. Al particles are nearly round in shape with very few have dumbbell or granular shape. The grain size of fine equiaxed and elongated Al particles are around 10 and 40 μm, respectively, with an average size of 30 μm.

Figure 3 represents the SEM images of MAed Fe<sub>60</sub>Al<sub>40</sub> powder for different duration of milling. During the initial phase of alloying, the equiaxed ductile material gets flattened into flaky and plate-like shapes by micro-forging action and results in cold welding by the repetitive action of collision in between balls on further milling [36].

An increase in average particle size was reported at this stage [8]. Particle sizes increased to 40 μm after 10 h of milling, which was higher than the as-received unprocessed powder mixture. On further milling, the hardness of composite powder particles increases because of strain hardening and gets broken under the impact of balls. This results in the more equiaxed grains and grain size was reduced to ~ 17 μm after 30 h of milling. Prolong milling ushers in a considerable reduction in grain size. Hardness and grain size were reached to the satiety level at this stage and alloying occurs at the microscopic level, which results in the development of solid solution intermetallics with nano-sized sub-grains. The grain size was abridged to 10 μm after 40 h of milling as shown in Fig. 4, and particles will be transferred into more regular and rounded in shape.

The structural developments in the Fe<sub>60</sub>Al<sub>40</sub> powder during the 40 h of MA were examined by XRD. Figures 5 and 6 reveal the XRD graphs of MAed powder for various periods of milling. Rupturing and alteration in phases of grains were detected throughout the MA. Thus, it was observed from the XRD graphs that with the prolonged milling, new phase formation occurred with the abolition of pure aluminum and iron powder.

The XRD peaks in Fig. 5 confirm that the diffraction peaks of aluminum powder, i.e., Al (200), Al (220), and Al (222), and iron powder, i.e., Fe (110), Fe (200), and Fe

**Table 1** Summary of process factors used during MA

Factors	Description
Milling bowl	Hardened steel (capacity 250 ml)
Milling balls size	Hardened steel balls of 5, 15, and 20 mm diameter
Elemental powders	Al (30 $\mu\text{m}$ ), Fe (35 $\mu\text{m}$ ) with 99% purity
PCA	2.5% Stearic acid ( $\text{CH}_3(\text{CH}_2)_{16}\text{COOH}$ )
BPR	10:1
Operating speed	195 rpm
Milling atmosphere	Argon gas (99.9% pure)

(211), shifted toward the lower diffraction angles, while odd Miller indices diffraction peaks of aluminum powder Al (111) and Al (311) are sovereign. The whole course of the transformation was demonstrated by the X-ray diffraction patterns as shown in Fig. 6.

On prolong milling, a gradual decline in the intensity of the crystalline peaks was observed and shift to the lower angle side with increasing milling time. After 10 h of milling the sharp-edged crystalline peaks of Al (111) and Al (311) were reduced considerably owing to the peak broadening and were ascribed to the reduction in crystallite size with proliferation in internal strains. However, diffraction peaks of iron were moved to a lesser diffraction angle. The results obtained from the XRD graphs listed in Table 2, it is obvious that the principal peaks of Al (111) and Fe (110) were gradually shifted to the lower side from  $2\theta = 44.47^\circ$  to  $2\theta = 44.087^\circ$  and  $2\theta = 38.218^\circ$  to  $2\theta = 37.843^\circ$ , respectively, for various milled time. This movement of peaks specifies the diffusion of Al atoms in the Fe lattice [37, 38].

Since the atomic radius of aluminum atoms (0.143 nm) was more than iron atoms (0.124 nm), diffusion of Al atoms in the Fe lattice leads to increase in the distance of

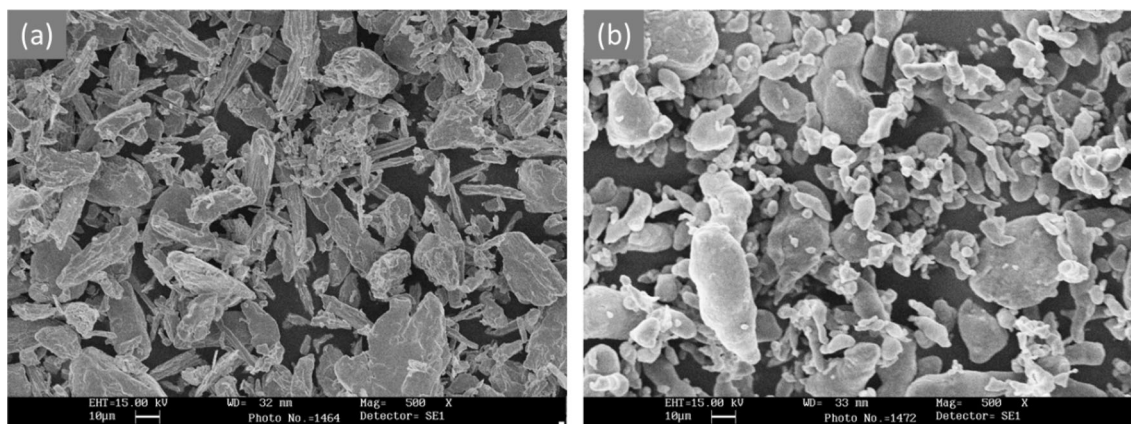
the atomic planes of iron which shift its peaks to lower angles and increase the lattice parameter. This results in the formation of the disordered solid solution of Fe(Al) intermetallic. The variation of lattice parameter of bcc phase after prolonged milling is represented in Fig. 7. The lattice parameter was determined using Nelson–Riley function [38]. After 10 h of milling, the lattice parameter was increased to 0.289 nm which was somewhat more than the un-milled pure Fe (0.2866 nm). After 40 h of milling the lattice parameter of Fe(Al) was found to be 0.293 nm. Similar type of result was also reported by Talischi et al. [39] and Panda et al. [40].

Figure 8 represents the variations in the crystallite size of the MAed powder for various milling times. The crystallite size of the MAed powder was measured with an XRD pattern using Debye–Scherrer’s formula [41] given in Eq. (1).

$$D_s = \frac{K\lambda}{\beta_D \cos \theta} \quad (1)$$

where  $\beta_D$  is the FWHM in radians,  $K$  is the Scherrer constant,  $D_s$  is the crystallite size,  $\lambda$  is the X-ray wavelength, and  $\theta$  is the peak positions in radians.

The obtained average crystallite size of the Al–Fe unprocessed mixture was 149 nm. The crystallite size after 10, 20, and 30 h of MA were found 81.56, 30.27, and 19.78 nm, respectively. After 40 h of MA, the resulting mean crystallite size was 18.2 nm that offers many new open reactive surfaces. The extended repetitive collision and exposure of new surfaces caused an exothermic reaction, which makes Al and Fe further responsive to the environmental gasses as well. Thus, it demands some inert environment to reduce the attack of the surrounding environment. The reduced grain size and fine dispersoids make MAed material stronger, harder, ductile, and wear-resistant. The broadening of the diffraction peaks after ball milling can be attributed to the refinement of the crystallite

**Fig. 2** SEM micrographs of a pure Iron b pure aluminum

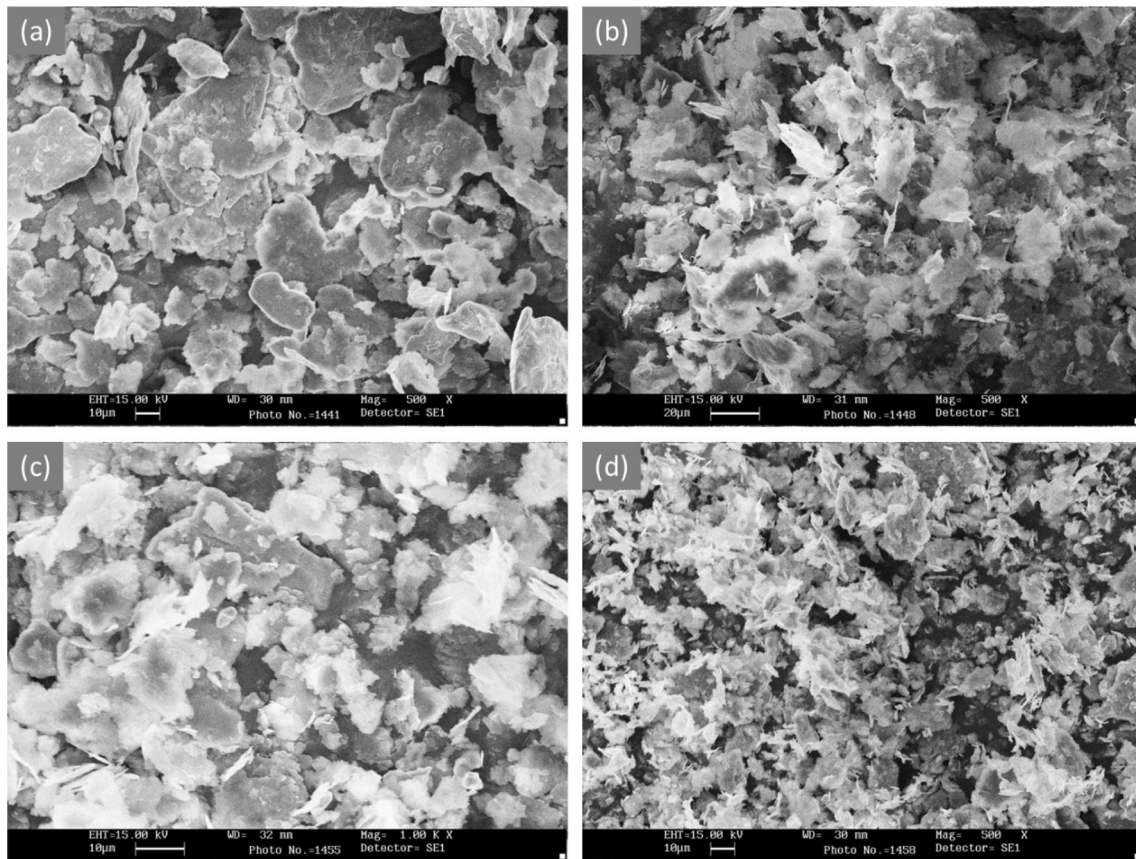


Fig. 3 SEM micrographs of MAed Fe<sub>60</sub>Al<sub>40</sub> powder milled for a 10 h, b 20 h, c 30 h, d 40 h

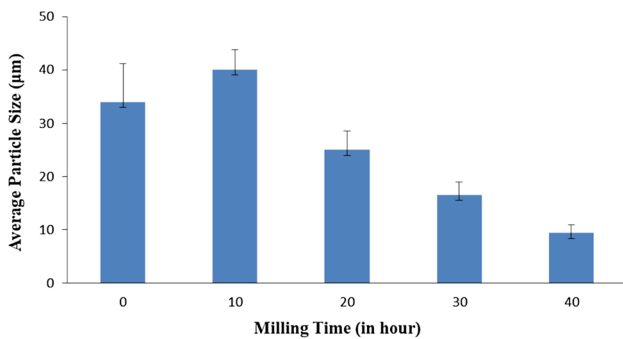


Fig. 4 Variations in average grain size with time during MA

size with an increase in internal strains. (Total broadening of the diffraction peaks is a sum of the broadening due to crystallite size and strain.) To separate the effect of crystallite size reduction from that of lattice strain, Williamson and Hall (W–H) approach has been adopted [42]. The strain  $\epsilon$  in a crystal lattice produces some broadening  $\beta_\epsilon$  of the diffraction lines and is given by Eq. (2)

$$\beta_\epsilon = 4\epsilon \tan \theta \tag{2}$$

where  $\theta$  is the peak positions in radians.

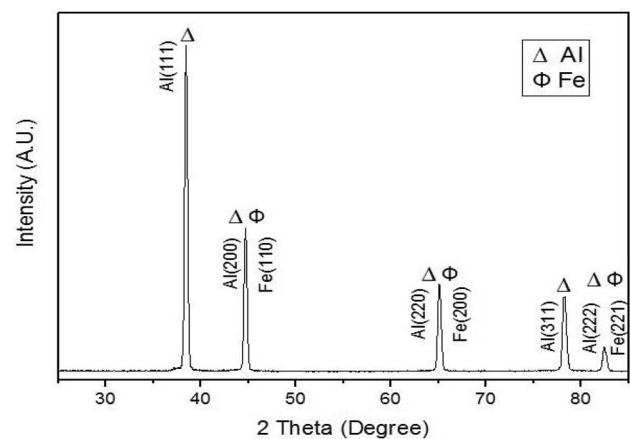
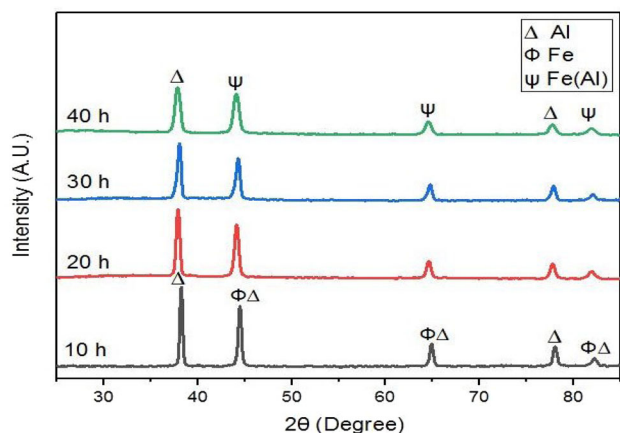


Fig. 5 XRD graph of pure Aluminum and Iron powder mixture

The calculated values of the lattice strain were measured with Williamson and Hall (W–H) approach and represented in Fig. 9. From the values of lattice strain, it was witnessed that the internal strain increases with the reduction of crystallite size due to work hardening after prolonged MA.

It was evident from the XRD peaks that, FWHM peaks were broadened with a reduction in peak intensity



**Fig. 6** XRD graphs of MAed  $\text{Fe}_{60}\text{Al}_{40}$  powder for various duration of milling

**Table 2** Principal peaks of Aluminum and Iron at  $2\theta$  for different milled time

Milling time (h)	The principal peak of Aluminum at $2\theta^\circ$	The principal peak of Iron at $2\theta^\circ$
10	38.218	44.47
20	38.017	44.27
30	37.882	44.13
40	37.843	44.087

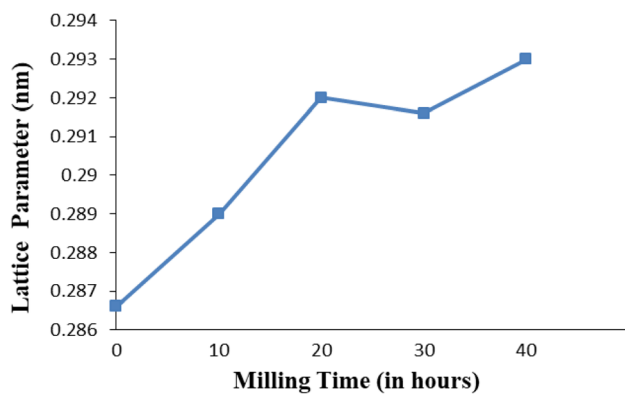


**Fig. 7** Variations in lattice parameter of Fe with milling time of MAed  $\text{Fe}_{60}\text{Al}_{40}$  powder

corresponding to increased milling time during the entire process. The value of FWHM witnessed after 10, 20, 30, and 40 h of milling were 0.312, 0.412, 0.495, and 0.533, respectively, at  $44.47^\circ$ . The broadening of the peaks expressed the decrease of the crystallite size of the powder. The related phenomena have also ensued for Fe(Al) peak at  $64.9^\circ$ ,  $78.06^\circ$ , and  $82.26^\circ$ .

The modification in structures of MAed powder has been attributed to the refinement of grains, solid solution dispersion, and growth of new phases. In the early stage of

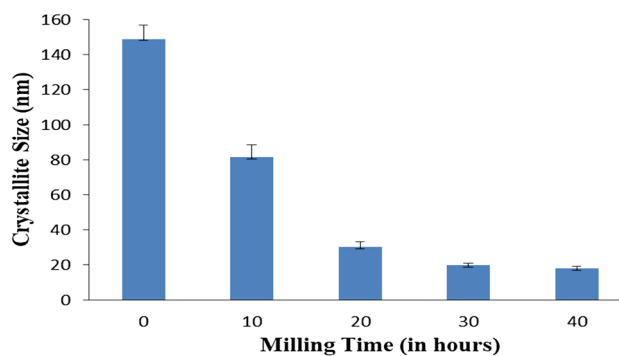


**Fig. 8** Variations in the crystallite size with milling time of MAed  $\text{Fe}_{60}\text{Al}_{40}$  powder

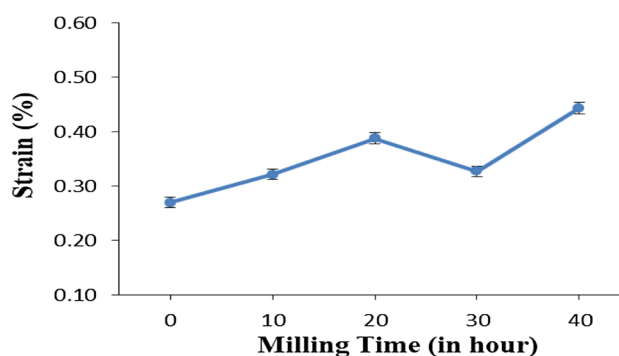


**Fig. 9** Variations in the lattice strain with milling time of MAed  $\text{Fe}_{60}\text{Al}_{40}$  powder

milling, no solid solutions were recognized among the MAed mixture. With the progress of milling widening of XRD peaks was detected, which indicates the distortion and rupturing of powders. Then shifting of the XRD peaks was observed, which indicates further dissolution of various elemental atoms, and at last development of new phases was detected by the construction of new peaks in the XRD graph.

The equilibrium solubility of aluminum in iron at room temperature was around 20% and almost nil for vice versa. However, by the MA process, approximately  $\sim 50\%$  aluminum can be dissolved in iron lattice while up to 10% of iron can be dissolved in aluminum [43]. The phase formation during MA occurs due to the solid-state diffusion of elemental powders. It was reported that aluminum atoms had a larger coefficient of diffusion than iron atoms and easily diffused in the iron lattice [44]. Apart from that, reduction in grain sizes of iron atoms and increase in the high-density crystal defects (dislocation and vacancy) were the other factors to improve the solid solubility of aluminum in iron. Diffusion of aluminum in iron attributes to an increased lattice parameter of iron and promotes the development of disordered Fe(Al) solid solution.

Therefore, substantial solid solubility was attained via the MA process. During the whole period of MA, no evidence of ordered FeAl and  $\text{DO}_3\text{-Fe}_3\text{Al}$  phases was observed on XRD traces. This may be due to the low rotational speed of mill or less milling time. Decrease in rotation speed retards the rate of formation of new phases, grain size to reduce, dislocations density to increase at a much lower rate and ultimately hindered the development of ordered FeAl and  $\text{DO}_3\text{-Fe}_3\text{Al}$  phases [36]. Since MA was performed in the hardened steel milling media, no contamination of mixed powder was witnessed owing to the wear in the milling medium as Fe and Al are comparatively much softer than hardened steel.

## Conclusion

The present study has observed the synthesis and characterization of Fe(Al) intermetallic compound with nanocrystalline grain. Nano-crystallite-disordered Fe(Al) intermetallic was efficaciously produced from the elemental powder mixture of iron and aluminum in the ratio of 3:2 by MA under inert argon medium. SEM micrographs exhibit the change of particle shape and size after every 10 h of mechanical alloying. Initially, the particle mixture flattened and with an increase of time, the cold welding followed by fracturing started and resulted in finer particle size. The average grain size reduced from 34 microns to 9.37 microns. The crystallite size reduced from 149 to 18.2 nm due to the refinement of grains. The internal strain also increased to 0.44% with the decrease of crystallite size. The new phases also formed with an increase in time. MA is an appropriate method to develop a solid solution-disordered phase of Fe(Al) under a controlled environment. SEM study report that the grain size of the MAed mixture was abridged to  $\sim 9 \mu\text{m}$  and crystallite size of about 18.2 nm after 40 h of continued milling.

**Funding** No financial grant was received from any funding agency.

## Declarations

**Conflict of interest** All authors declare that they have no conflict of interest.

## References

- N.S. Stoloff, C.T. Liu, S.C. Deevi, Emerging applications of intermetallics. *Intermetallics* **8**, 1313–1320 (2000)
- P.F. Tortorelli, J.H. DeVan, Behavior of iron aluminides in oxidizing and oxidizing/sulfidizing environments. *Mater. Sci. Eng. A* **A153**(1–2 pt 2), 573–577 (1992). [https://doi.org/10.1016/0921-5093\(92\)90253-W](https://doi.org/10.1016/0921-5093(92)90253-W)
- I. Baker, P.R. Munroe, Mechanical properties of FeAl. *Int. Mater. Rev.* **42**(5), 181–205 (1997). <https://doi.org/10.1179/imr.1997.42.5.181>
- S.C. Deevi, V.K. Sikka, C.T. Liu, Processing, properties, and applications of nickel and iron aluminides. *Prog. Mater. Sci.* **42**(1–4), 177–192 (1997). [https://doi.org/10.1016/S0079-6425\(97\)00014-5](https://doi.org/10.1016/S0079-6425(97)00014-5)
- S.C. Deevi, V.K. Sikka, Nickel and iron aluminides: an overview on properties, processing, and applications. *Intermetallics* **4**(5), 357–375 (1996). [https://doi.org/10.1016/0966-9795\(95\)00056-9](https://doi.org/10.1016/0966-9795(95)00056-9)
- M. Krasnowski, T. Kulik, Nanocrystalline FeAl intermetallic produced by mechanical alloying followed by hot-pressing consolidation. *Intermetallics* **15**(2), 201–205 (2007). <https://doi.org/10.1016/j.intermet.2006.05.008>
- V. K. Sikka, *Intermetallic-based high-temperature materials*. in NACE International Corrosion Conference Series, vol. 1999, no. 1, 1999
- D. Oleszak, P.H. Shingu, Mechanical alloying in the FeAl system. *Mater. Sci. Eng. A* **181–182**(C), 1217–1221 (1994). [https://doi.org/10.1016/0921-5093\(94\)90834-6](https://doi.org/10.1016/0921-5093(94)90834-6)
- M. Krasnowski, A. Grabias, T. Kulik, Phase transformations during mechanical alloying of Fe-50% Al and subsequent heating of the milling product. *J. Alloys Compd.* **424**(1–2), 119–127 (2006). <https://doi.org/10.1016/j.jallcom.2005.12.077>
- S. Enzo et al., X-ray powder diffraction and Mössbauer study of nanocrystalline Fe-Al prepared by mechanical alloying. *Acta Mater.* **44**(8), 3105–3113 (1996). [https://doi.org/10.1016/1359-6454\(95\)00431-9](https://doi.org/10.1016/1359-6454(95)00431-9)
- K. Wolski, G. Le Caër, P. Delcroix, R. Fillit, F. Thévenot, J. Le Coze, Influence of milling conditions on the FeAl intermetallic formation by mechanical alloying. *Mater. Sci. Eng. A* **207**(1), 97–104 (1996). [https://doi.org/10.1016/0921-5093\(96\)80006-2](https://doi.org/10.1016/0921-5093(96)80006-2)
- B. Huang, K.N. Ishihara, P.H. Shingu, Metastable phases of Al-Fe system by mechanical alloying. *Mater. Sci. Eng. A* **231**(1–2), 72–79 (1997). [https://doi.org/10.1016/S0921-5093\(97\)00041-5](https://doi.org/10.1016/S0921-5093(97)00041-5)
- D.A. Eelman, J.R. Dahn, G.R. MacKay, R.A. Dunlap, An investigation of mechanically alloyed Fe-Al. *J. Alloys Compd.* **266**(1–2), 234–240 (1998). [https://doi.org/10.1016/S0925-8388\(97\)00508-2](https://doi.org/10.1016/S0925-8388(97)00508-2)
- M.A. Morris-Muñoz, A. Dodge, D.G. Morris, Structure, strength and toughness of nanocrystalline FeAl. *Nanostructured Mater.* **11**(7), 873–885 (1999). [https://doi.org/10.1016/S0965-9773\(99\)00385-2](https://doi.org/10.1016/S0965-9773(99)00385-2)
- J.S. Benjamin, Mechanical alloying. *Sci. Am. INC* **234**(5), 40–48 (1976)
- C. Suryanarayana, E. Ivanov, V.V. Boldyrev, The science and technology of mechanical alloying. *Mater. Sci. Eng. A* **304–306**(1–2), 151–158 (2001). [https://doi.org/10.1016/S0921-5093\(00\)01465-9](https://doi.org/10.1016/S0921-5093(00)01465-9)
- Y. Liu, W. Liu, Mechanical alloying and spark plasma sintering of the intermetallic compound Ti50Al50. *J. Alloys Compd.* **440**(1–2), 154–157 (2007). <https://doi.org/10.1016/j.jallcom.2006.09.060>
- S. Çam, V. Demir, D. Özyürek, Wear behaviour of A356/TiAl3 in situ composites produced by mechanical alloying. *Metals (Basel)* **6**(2), 25–27 (2016). <https://doi.org/10.3390/met6020034>
- M. Zadra, Mechanical alloying of titanium. *Mater. Sci. Eng. A* **583**, 105–113 (2013). <https://doi.org/10.1016/j.msea.2013.06.064>
- L. Dias, B. Trindade, C. Coelho, S. Patankar, C. Draney, F.H. Sam Froes, Ti-Mg-Si alloys produced by non-equilibrium processing methods: mechanical alloying and sputtering. *Mater. Sci. Eng. A* **364**(1–2), 273–280 (2004)
- M. Wang, H.N. Han, H.S. Chung, Y.B. Chun, J. Jang, Microstructural evolution of oxide and nitride dispersed nickel-based alloy powders. *Met. Mater. Int.* **25**(1), 140–146 (2019). <https://doi.org/10.1007/s12540-018-0176-6>

22. B.S. Murty, S. Ranganathan, Novel materials synthesis by mechanical alloying/milling. *Int. Mater. Rev.* **43**(3), 101–141 (1998). <https://doi.org/10.1179/imr.1998.43.3.101>
23. M.K. Yadav, A.N. Siddiquee, Z.A. Khan, Characterization of Ti–Al intermetallic synthesized by mechanical alloying process. *Met. Mater. Int.* (2020). <https://doi.org/10.1007/s12540-019-00603-w>
24. S. Alamolhoda, S. Heshmati-Manesh, A. Ataie, A. Badiei, Role of process control agents on milling behavior of Al and TiO<sub>2</sub> powder mixture to synthesize TiAl/Al<sub>2</sub>O<sub>3</sub> nano composite. *Int. J. Mod. Phys. Conf. Ser.* **05**, 638–645 (2012). <https://doi.org/10.1142/s2010194512002577>
25. M. Abd Elhamid, M.M. Emara, H.G. Salem, Influence of mixing technique on the mechanical properties and structural evolution of Al–NiAl composites. *J. Mater. Eng. Perform.* **23**(10), 3425–3435 (2014)
26. H. Shi, D. Guo, Y. Ouyang, Structural evolution of mechanically alloyed nanocrystalline FeAl intermetallics. *J. Alloys Compd.* **455**(1–2), 207–209 (2008). <https://doi.org/10.1016/j.jallcom.2007.01.079>
27. Z.H. Chin, T.P. Perng, In situ observation of combustion to form TiN during ball milling Ti in nitrogen. *Appl. Phys. Lett.* **70**(18), 2380–2382 (1997). <https://doi.org/10.1063/1.119084>
28. M.K.-V.D.L. Beke, Phase transitions in Cu–Sb systems induced by ball milling. *Mater. Sci. Forum* **225–227**, 465–470 (1996). <https://doi.org/10.1557/mrs2002.257>
29. S.N.A. Muttalib, N. Othman, Effect of ball milling parameters on properties of attapulgite filled natural rubber composite. *Procedia Chem.* **19**, 381–387 (2016). <https://doi.org/10.1016/j.proche.2016.03.027>
30. H. Ghayour, M. Abdellahi, M. Bahmanpour, Optimization of the high energy ball-milling: modeling and parametric study. *Powder Technol.* **291**, 7–13 (2016). <https://doi.org/10.1016/j.powtec.2015.12.004>
31. E. Basiri Tochaee, H.R. Madaah Hosseini, S.M. Seyed Reihani, On the fracture toughness behavior of in-situ Al–Ti composites produced via mechanical alloying and hot extrusion. *J. Alloys Compd.* **681**, 12–21 (2016)
32. F.G. Cuevas, J. Cintas, J.M. Montes, J.M. Gallardo, Al–Ti powder produced through mechanical alloying for different times. *J. Mater. Sci.* **41**(24), 8339–8346 (2006). <https://doi.org/10.1007/s10853-006-1029-0>
33. C. Suryanarayana, Mechanical alloying and milling. *Mech. Alloy. Milling* **46**, 1–184 (2001). <https://doi.org/10.4150/kpmi.2006.13.5.371>
34. L. Takacs, M. Pardavi-Horvath, Nanocomposite formation in the Fe<sub>3</sub>O<sub>4</sub>–Zn system by reaction milling. *J. Appl. Phys.* **75**(10), 5864–5866 (1994). <https://doi.org/10.1063/1.355543>
35. L. Zhang, X. Guo, Microstructural evolution, thermal stability and microhardness of the Nb–Ti–Si-based alloy during mechanical alloying. *Metals (Basel)* **8**(6), 403 (2018). <https://doi.org/10.3390/met8060403>
36. M.H. Enayati, M. Salehi, Formation mechanism of Fe<sub>3</sub>Al and FeAl intermetallic compounds during mechanical alloying. *J. Mater. Sci.* **40**(15), 3933–3938 (2005). <https://doi.org/10.1007/s10853-005-0718-4>
37. J.B. Al-Dabbagh, R.M. Tahar, M. Ishak, S.A. Harun, Structural and phase formation of TiAl alloys synthesized by mechanical alloying and heat treatment. *Int. J. Nanoelectron. Mater.* **8**(1), 23–32 (2015)
38. M. G. Norton, C. Suryanarayana, X-ray diffraction: a practical approach. (1998)
39. A. Samadi, L.A. Talischi, Structural characterization and ordering transformation of mechanically alloyed nanocrystalline Fe–28Al. *Powder Met. Rev.* **6**(2), 353–358 (2016)
40. D. Panda, P. Bhuyan, L. Kumar, S.N. Alam, Synthesis of Fe<sub>3</sub>Al intermetallic compound by mechanical alloying. *Arab. J. Sci. Eng.* **42**(10), 4427–4437 (2017). <https://doi.org/10.1007/s13369-017-2526-y>
41. T.T. Bui, X.Q. Le, D.P. To, V.T. Nguyen, Investigation of typical properties of nanocrystalline iron powders prepared by ball milling techniques. *Adv. Nat. Sci. Nanosci. Nanotechnol.* **4**(4), 045003 (2013). <https://doi.org/10.1088/2043-6262/4/4/045003>
42. G.K. Williamson, W.H. Hall, X-ray line broadening from filed aluminium and wolfram. *Acta Metall* **1**(1), 22–31 (1953). [https://doi.org/10.1016/0001-6160\(53\)90006-6](https://doi.org/10.1016/0001-6160(53)90006-6)
43. S.S. Nayak, M. Wollgarten, J. Banhart, S.K. Pabi, B.S. Murty, Nanocomposites and an extremely hard nanocrystalline intermetallic of Al–Fe alloys prepared by mechanical alloying. *Mater. Sci. Eng. A* **527**(9), 2370–2378 (2010). <https://doi.org/10.1016/j.msea.2009.12.044>
44. A. Olszówka-Myalska, W. Maziarz, Microstructural analysis of iron aluminide formed by self-propagating high-temperature synthesis mechanism in aluminium matrix composite. *J. Microsc.* **224**(1), 1–3 (2006). <https://doi.org/10.1111/j.1365-2818.2006.01635.x>

**Publisher's Note** Springer Nature remains neutral with regard to jurisdictional claims in published maps and institutional affiliations.